

# PCCP

Accepted Manuscript



This is an *Accepted Manuscript*, which has been through the Royal Society of Chemistry peer review process and has been accepted for publication.

*Accepted Manuscripts* are published online shortly after acceptance, before technical editing, formatting and proof reading. Using this free service, authors can make their results available to the community, in citable form, before we publish the edited article. We will replace this *Accepted Manuscript* with the edited and formatted *Advance Article* as soon as it is available.

You can find more information about *Accepted Manuscripts* in the [Information for Authors](#).

Please note that technical editing may introduce minor changes to the text and/or graphics, which may alter content. The journal's standard [Terms & Conditions](#) and the [Ethical guidelines](#) still apply. In no event shall the Royal Society of Chemistry be held responsible for any errors or omissions in this *Accepted Manuscript* or any consequences arising from the use of any information it contains.

**Photocatalytic degradation of methylene blue with nanocomposite system:****synthesis, photocatalysis and degradation pathways**

Shengjie Xia<sup>a</sup>, Lianyang Zhang<sup>a</sup>, Guoxiang Pan<sup>b</sup>, Pingping Qian<sup>a</sup>, Zheming Ni<sup>a,\*</sup>

<sup>a</sup>*Department of Chemistry, College of Chemical Engineering, Zhejiang University of Technology, Hangzhou 310032, P R China*

<sup>b</sup>*Department of Materials Chemistry, School of Life Science, Huzhou Teachers college, Huzhou, 313000, P R China*

---

\* Corresponding author.

E-mail: [jchx@zjut.edu.cn](mailto:jchx@zjut.edu.cn), [nzm@zjut.edu.cn](mailto:nzm@zjut.edu.cn)

Telephone number: 086-0571-88320373

**Abstract:**

Three different composites, including calcined FeOOH supported ZnAl layered double hydroxides (FeOOH-LDO), calcined ZnAl layered double hydroxides (ZnAl-LDO) and calcined ZnFeAl layered double hydroxides (ZnFeAl-LDO), were synthesized by sol-gel method, and their activity for visible light photocatalytic degradation of methylene blue (MB) was also studied. Composites were characterized by PXRD, SEM, and BET techniques, confirming the formation of good crystal structure. The degradation activity performance of MB degradation is following the order: FeOOH-LDO (~95%) > ZnFeAl-LDO (~60%) > ZnAl-LDO (~23%). In addition, a possible photocatalytic degradation reaction mechanism on MB has also been presumed. Moreover, Frontier electron densities on atoms of MB were calculated, which is in satisfactory agreement with the possible mechanism.

**Keywords:** Photocatalysis; Layered double hydroxides; FeOOH; Degradation pathways

## 1. Introduction

Dye compounds being released from textile effluents are a dramatic source of non-aesthetic pollution and eutrophication in the aquatic ecosystems [1]. Techniques for the removal of dyes have been intensively studied recently because the international environmental standards are becoming more and more stringent [2]. Among these technologies, the methods based on chemical (chlorination, ozonation), physical (adsorption etc.) and biological theories (biodegradation) have been applied in reality [3–7]. Photocatalysis [8,9], used as a potential technology to treat the dye process disposal, has brought excellent result to most of the dye wastewaters. At present, the widely used semiconductive photocatalysts (such as  $\text{TiO}_2$  [10,11] and  $\text{ZnO}$  [12–14]), have the disadvantages such as high band gaps, low photo-electron transfer efficiency and low recycling rates. Therefore, the searching for low band gap materials used as photocatalysts is needed to improve the utilization of sunlight for the remove of dye compounds from wastewaters.

Layered double hydroxides (LDHs) is a class of lamellar solid with the general formula of  $[\text{M}^{2+}_{1-x}\text{M}^{3+}_x(\text{OH})_2]^{x+}(\text{A}^{n-})_{x/n} \cdot m\text{H}_2\text{O}$ , where  $\text{M}^{2+}$  is  $\text{Mg}^{2+}$ ,  $\text{Co}^{2+}$ ,  $\text{Zn}^{2+}$ , etc. and  $\text{M}^{3+}$  is  $\text{Al}^{3+}$ ,  $\text{Cr}^{3+}$ ,  $\text{Fe}^{3+}$ , etc.  $\text{A}^{n-}$  is interlayer anion, such as  $\text{CO}_3^{2-}$ ,  $\text{NO}_3^-$ ,  $\text{Cl}^-$  and  $\text{OH}^-$  [15,16]. LDH have been used as catalysts and catalyst precursors in a variety of chemical reactions [5,17]. In addition, the composites of bimetallic or trimetallic oxide with high specific surface area, special micro-structure and high pH values could be formed after calcinations of layered double hydroxides. Therefore, that materials have been successfully employed in many acid-base catalyzed reactions

[18]. Moreover, the second or third metals could be highly dispersed and doped into the LDH materials, thus, the photocatalytic property of these composites could be greatly improved. Particularly, nanocomposite materials calcined from Fe and Zn based layered double hydroxides under special temperature, would yield  $\text{ZnFe}_2\text{O}_4$  and other oxides (such as  $\text{ZnO}$ ,  $\text{Al}_2\text{O}_3$ ). It is well known that,  $\text{ZnFe}_2\text{O}_4$  with a spinel structure has been widely studied recently due to its photochemical stability, chemical stability and visible light sensitivity [19,20]. As a semiconductor with a narrow band gap value of 1.86 eV,  $\text{ZnFe}_2\text{O}_4$  could be an outstanding candidate for visible light photocatalyst. Recently,  $\text{ZnFe}_2\text{O}_4$  has been coupled with various high band gap semiconductors to delay the fast electron/hole recombination which causes the quick activity decrease of photocatalysts. In recent references, Yu [21] showed that  $\text{ZnFe}_2\text{O}_4$  modified with CdS nanorods was highly efficient and visible light responsive, it was also photochemically stable and magnetically recyclable for hydrogen generation. Hamze [22] synthesized  $\text{ZnO-ZnFe}_2\text{O}_4$  composite photocatalyst on activated carbon support which was further applied for the chromium ions removal from a raw tannery effluent; the conversion of total chromium was as high as 91% in 120 min.

In this work, we have synthesized there calcined composite, including  $\text{FeOOH/ZnAl-LDO}$ ,  $\text{ZnAl-LDO}$  and  $\text{ZnFeAl-LDO}$  by sol-gel method, and studied their activity for visible light photocatalytic degradation of methylene blue. All the materials have shown good crystal structure based on the results of PXRD, SEM, and BET analysis. Moreover, the degradation rate and the regeneration of materials

composite have also been investigated. In addition, the photocatalytic degradation pathways and the possible intermediate products are also discussed.

## 2. Experimental

### 2.1 Materials

Methylene blue ( $C_{16}H_{18}ClN_3S \cdot 3H_2O$ , abbreviated as MB here) and other reagents were all analytical grade (AR) and used without further purification. MB was purchased from Shanghai SSS Reagent Co. Ltd. (China), and its dilutions were prepared by dissolving MB in deionized water; Reagents were all from Sinopharm Chemical Reagent Co. Ltd. (China); Deionized water was boiled to decarbonate before employing in all synthesis steps.

### 2.2 Preparation of samples

#### 2.2.1 Synthesis of ZnAl-LDHs and oxides

The LDHs with Zn:Al molar ratio 3 was prepared by a coprecipitation method. Aqueous solution of NaOH (32.0 g, 0.8 mol) and  $Na_2CO_3$  (5.3 g, 0.05 mol), and the other 150 mL solution of  $Zn(NO_3)_2 \cdot 6H_2O$  (89.2 g, 0.3 mol) and  $Al(NO_3)_3 \cdot 9H_2O$  (37.6 g, 0.1 mol), were added dropwise into 200 mL deionized water with vigorous stirring at 65 °C and pH 9–10. The resultant slurry was aged at 65 °C for 24 h, and then centrifuged and washed with deionized water until the pH = 7, after it was dried in vacuo at 85 °C for 18 h, the product was crashed and passed through an 100-mesh sieve. The prepared catalysts precursors were designated as ZnAl-LDHs.

The dried ZnAl-LDHs were further calcined in air at 500 °C for 4 h, with a heating rate of 5 °C/min, the calcined product was ZnAl-LDO.

### 2.2.2 Synthesis of ZnFeAl-LDHs and oxides

NaOH (32.0 g, 0.8 mol) and Na<sub>2</sub>CO<sub>3</sub> (5.3 g, 0.05 mol) were dissolved in 150 mL deionized water (solution A). Zn(NO<sub>3</sub>)<sub>2</sub>·6H<sub>2</sub>O (89.2 g, 0.3 mol), Fe(NO<sub>3</sub>)<sub>3</sub>·9H<sub>2</sub>O (20.2 g, 0.05 mol) and Al(NO<sub>3</sub>)<sub>3</sub>·9H<sub>2</sub>O (18.8 g, 0.05 mol) were dissolved in 150 mL deionized water (solution B). Solution A and solution B were added dropwise in 200 mL deionized water with vigorous stirring at 65 °C and pH 9–10. The resultant slurry was aged at 65 °C for 24 h, and then centrifuged and washed with deionized water until the pH = 7, after it was dried in vacuo at 85 °C for 18 h, then crashed and passed through an 100-mesh sieve. The prepared catalysts precursors were designated as ZnFeAl-LDHs. The dried ZnFeAl-LDHs were further calcined in air at 500 °C for 4 h, with a heating rate of 5 °C/min, giving the calcined product ZnFeAl-LDO.

### 2.2.3 Synthesis of FeOOH/ZnAl-LDHs composites and calcined product

The FeOOH (8.48 g) and deionized water (200 mL) were added into 500 mL flask under constant stirring at 65 °C for 5 h. Then one solution (150 mL) containing a mixture of NaOH (32.0 g, 0.8 mol) and Na<sub>2</sub>CO<sub>3</sub> (5.3 g, 0.05 mol), and the other solution with (150 mL) Zn(NO<sub>3</sub>)<sub>2</sub>·6H<sub>2</sub>O (89.2 g, 0.3 mol) and Al(NO<sub>3</sub>)<sub>3</sub>·9H<sub>2</sub>O (37.6 g, 0.1 mol), were added dropwise in 200 mL of FeOOH solution under vigorous stirring at 65 °C and pH 9–10. The resultant slurry was aged at 65 °C for 24 h, and then centrifuged and washed with deionized water until the pH = 7, after it was dried in vacuo at 85 °C for 18 h, then crashed and passed through an 100-mesh sieve. The prepared catalysts precursors are designated as FeOOH/ZnAl-LDHs (labeled as FeOOH-LDHs). The dried FeOOH/ZnAl-LDHs were further calcined in air at

500 °C for 4 h, with a heating rate of 5 °C/min, giving the calcined product FeOOH/ZnAl-LDHs (labeled as FeOOH-LDO). In addition, FeOOH was also calcined in air at 500 °C for 4 h, and obtained calcined product which was abbreviated as CF.

### 2.3 Characterizations

Powder X-ray diffraction (PXRD) was recorded on a Beijing Puxi XRD-6 type diffractometer using Cu  $K_{\alpha}$  radiation ( $\lambda = 0.15418$  nm) at 20 mA and 36 kV, with a scanning rate of 4°/min and  $2\theta$  angle ranging from 5 to 80 °.

Fourier transform infrared (FT-IR) of the samples were studied using a NICOLET 6700 spectrometer in the wavenumber range of 400–4000  $\text{cm}^{-1}$ . The samples were mixed with KBr and compressed into pellet for the measurement.

SEM analysis was carried out in a Hitachi SU1510 ESEM with an acceleration voltage of 15 kV. TEM was recorded on a Hitachi HT-7700 to examine the morphologies, lattice fringes and crystal boundaries of the samples.

UV-Vis DRS of the samples were measured on a UV-Vis diffuse reflection spectrum (Model-2550, Shimadzu) equipped with an integrating sphere attachment using BaSO<sub>4</sub> as background, the spectra was recorded in the range of 200–800 nm.

### 2.4 Photocatalytic reactions

The photocatalytic activity of catalysts was monitored by degradation of methylene blue (MB) under irradiation with visible light using a 500 W xenon lamp at the room temperature (about 25 °C). Running water was circulated through the jacket to maintain constant temperature of the reaction system, the solution was stirred

magnetically. Typically, a mixture of 50 ml of MB (3.0 mg/L) solution and 175 mg of catalyst was mixed and vigorously stirred for 30 min to establish an adsorption/desorption equilibrium in darkness. Then the reaction solution was stirred under visible-light irradiation for several hours. At given time intervals, 2 ml aliquots were sampled and filtered to remove the solid phase. The filtrates were tested by measuring the absorbance at 446 nm by using UV-Vis spectrophotometer and the blank reaction was also carried out by the same procedure without adding any LDHs catalyst.

### 3. Results and discussion

#### 3.1 Structural characteristics of LDHs

Figure 1A shows the powder XRD patterns of ZnAl-LDHs, ZnFeAl-LDHs, FeOOH and FeOOH-LDHs. Strong reflection peaks at (003), (006), (009), (110) and (113) were observed in the three samples (ZnAl-LDHs, ZnFeAl-LDHs and FeOOH-LDHs) which can be indexed to typical LDH materials [23–24]. Moreover, according to the powder XRD patterns of ZnAl-LDHs, ZnFeAl-LDHs and FeOOH-LDHs, the interlayer distance ( $d_{003}$ ) are 0.77 nm ( $2\theta=11.58^\circ$ ), 0.79 nm ( $2\theta=11.26^\circ$ ) and 0.76 nm ( $2\theta=11.64^\circ$ ), respectively. In addition, after composition of FeOOH and ZnAl-LDHs, several extra diffraction peaks, including (012), (104), (110) and (113) of FeOOH, were emerged in the XRD pattern of FeOOH-LDHs, confirming the formation of FeOOH-LDHs composite.

Furthermore, as expected, upon calcination, the XRD pattern of ZnAl-LDO, ZnFeAl-LDO, FeOOH-LDO and CF composites (Figure 1B) showed that layered structure of the original LDHs was completely destroyed and appear  $\text{Al}_2\text{O}_3$ , ZnO,  $\text{Fe}_2\text{O}_3$  and  $\text{ZnAl}_2\text{O}_4$  peaks, while FeOOH-LDO has the extra  $\text{ZnFe}_2\text{O}_4$  peaks [21]. It suggests a complete decomposition of the original LDHs and the formation of ZnAl-LDO, ZnFeAl-LDO, FeOOH-LDO and CF composites.

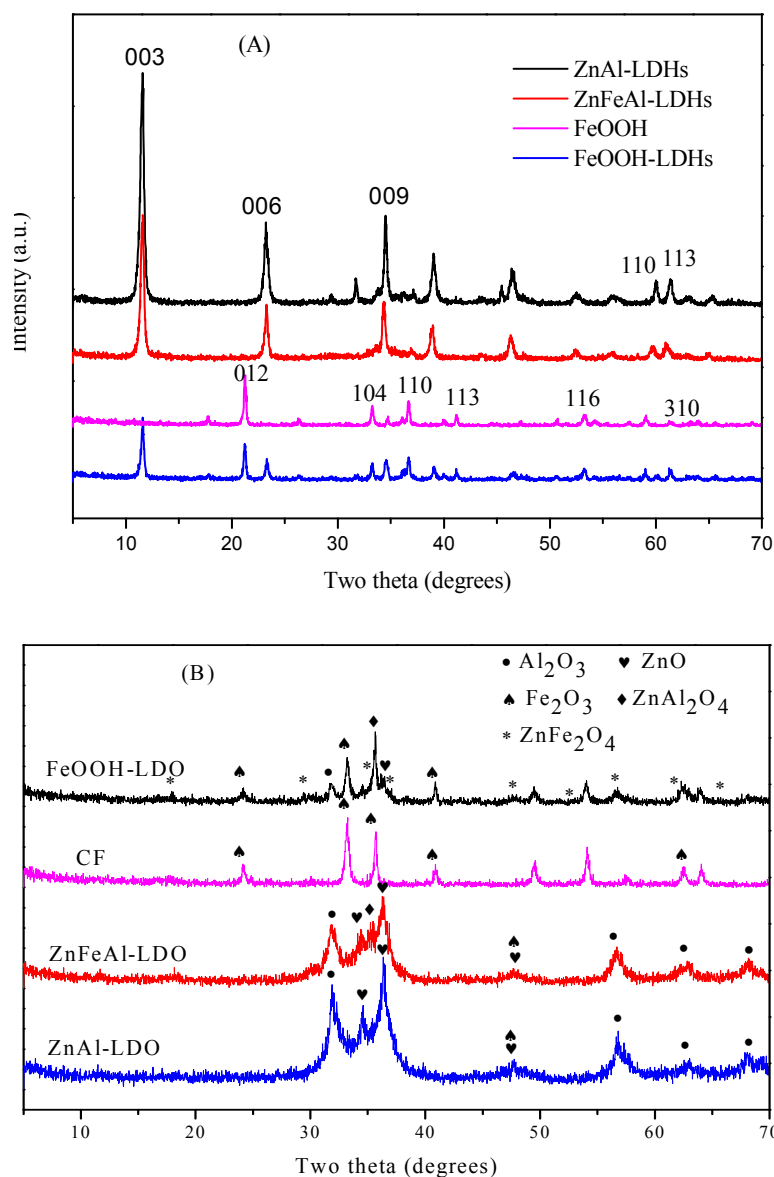


**Figure 1** (A) Power XRD patterns for ZnAl-LDHs, ZnFeAl-LDHs, FeOOH and FeOOH-LDHs; (B) Power XRD patterns for ZnAl-LDO, ZnFeAl-LDO, CF and FeOOH-LDO.

The SEM coupled with EDX image of the FeOOH, CF, FeOOH-LDHs and FeOOH-LDO are shown in Figure 2. As we can see from Figure 2A, FeOOH was a rod with the length of 10 – 20  $\mu\text{m}$ . After the FeOOH was calcined at 500  $^{\circ}\text{C}$  (labeled CF), the rod morphology was disappeared (Figure 2B). On the other hand, Figure 2C and Figure 2E show that the FeOOH-LDHs sample was consisted of rod and hierarchical structure, it further tells that FeOOH-LDHs sample with morphology feature of LDH and FeOOH was successfully synthesized. The SEM of FeOOH-LDO (FeOOH-LDHs after calcined at 500  $^{\circ}\text{C}$ ) shown in Figure 2D could reveal the information that the rod and hierarchical structure of FeOOH-LDHs were both disappeared, and nano-particles were obtained. In addition, The energy-dispersive X-ray spectrometry (EDX) analysis of the FeOOH-LDO (Figure 2F) shows the presence of Zn, Fe, Al, C and O with a Zn/(Fe+Al) molar ratio of  $\sim 0.89$ .

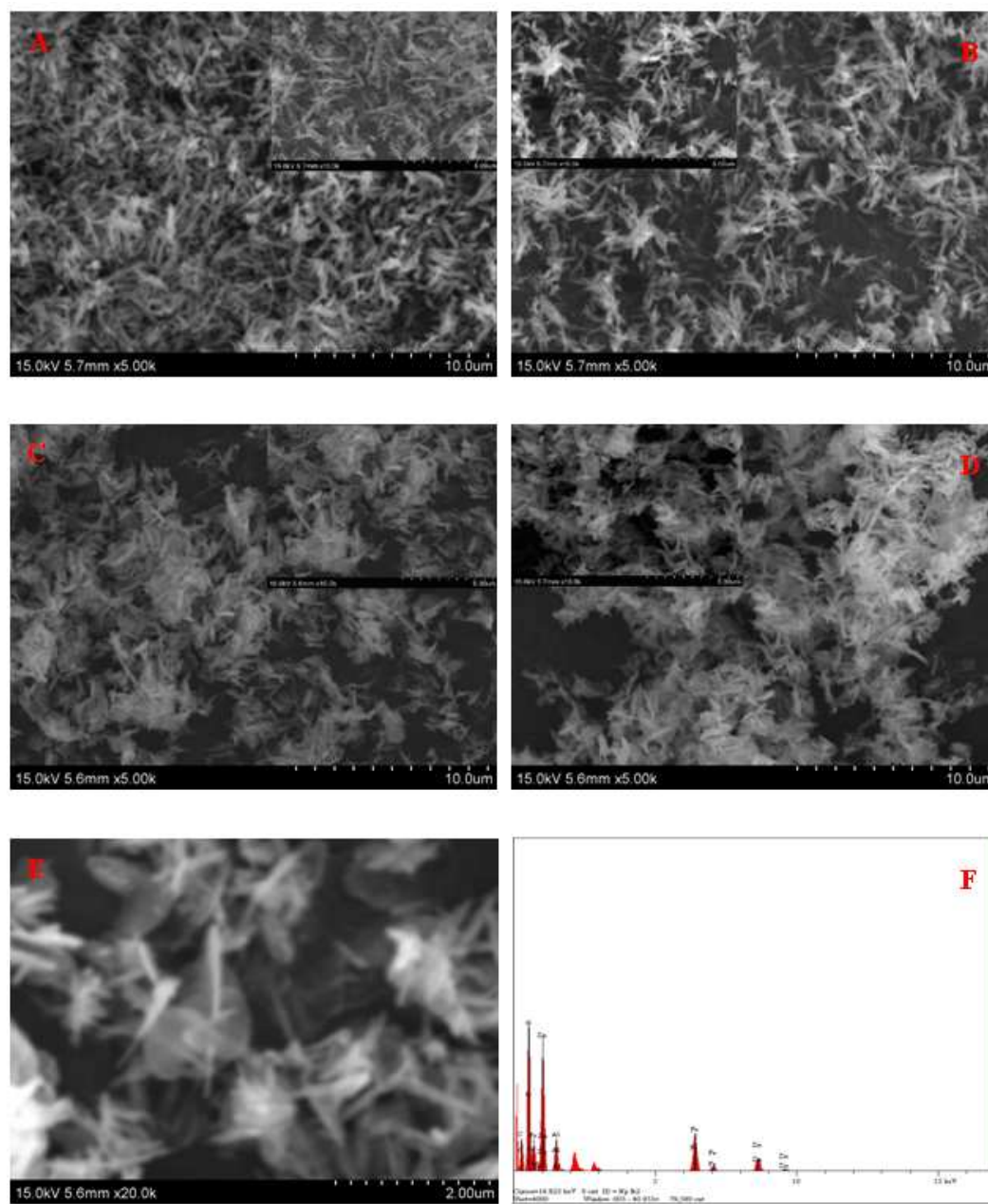


**Figure 2** SEM images for FeOOH (A), CF (B), FeOOH-LDHs (C) and FeOOH-LDO (D). FeOOH-LDHs with high-magnification (E). The corresponding EDX spectrum of the FeOOH-LDO (F).

For further study of the structure parameter of FeOOH-LDO composite, nitrogen sorption measurement was carried out. The shape of the isotherm was of type IV with

a broad H3 type hysteresis loop attributed to presence of mesopores, according to the IUPAC classification [25]. This result is further confirmed by the corresponding wide distribution of pore size in Figure 3 inset (maximum at 26 nm). The measured surface area for FeOOH–LDO is 18.74 m<sup>2</sup>/g.

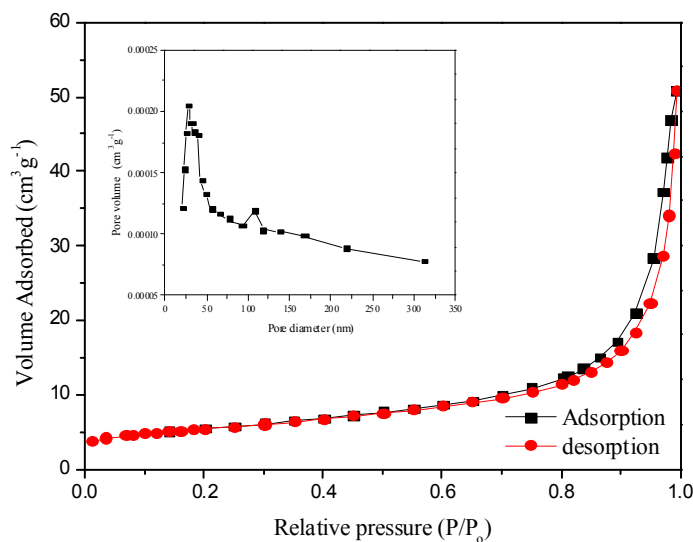
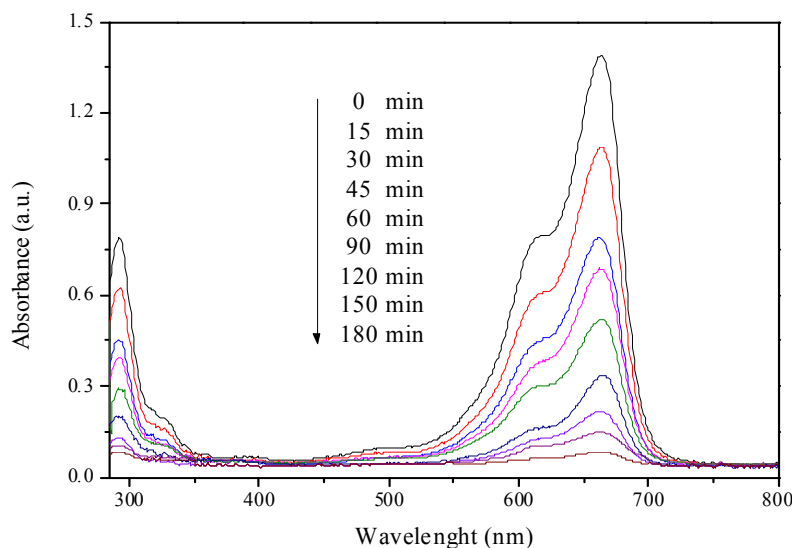


**Figure 3** N<sub>2</sub> sorption isotherms and pore size distribution of FeOOH–LDO.

### 3.2 Photocatalytic activities

The relationship between absorbance and irradiation time of MB degradation using FeOOH–LDO composite under visible light radiation was shown in Figure 4. The strong absorption bands of MB located at  $\lambda = 293$  nm and  $\lambda = 664$  nm decreases gradually upon increasing irradiation time and the absorbance of MB was about zero after 180 min of irradiation for FeOOH–LDO catalyst. MB solution color changed into nearly transparent during the degradation process. In addition, the strong

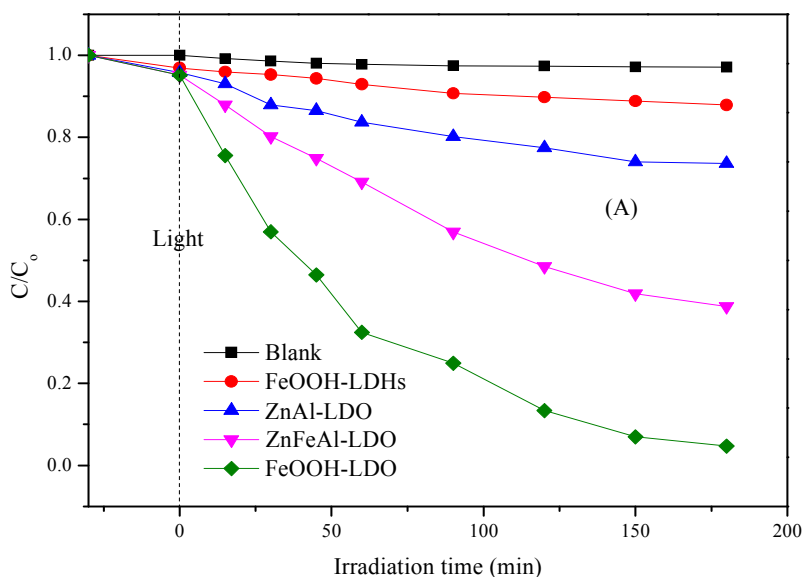
absorption bands of MB were not shifted, indicating that the degradation of MB is due to chromophores being destroyed [26].



**Figure 4** Absorption changes of MB during the photo-degradation process over FeOOH-LDO catalyst under visible-light irradiation.

The photocatalytic behavior of FeOOH-LDO catalyst was further evaluated by a comparison study with the performance of ZnFeAl-LDO, ZnAl-LDO and CF, as shown in Figure 5A. The decomposed amount of MB was calculated using  $C/C_0$ , where  $C$  and  $C_0$  are the absorbance intensity of the sample at time interval concentration and the initial concentration, respectively. The percentage of adsorption was 3% for MB. All catalysts (FeOOH-LDO, ZnFeAl-LDO, ZnAl-LDO and CF) exhibited photocatalytic activity for MB degradation under visible-light irradiation. The decomposition of MB by the FeOOH-LDO reached ~95% over 180 min,

compared to ~60%, ~23% and ~ 10% by the degradation samples with ZnFeAl-LDO, ZnAl-LDO and CF respectively. In addition, from Fig.5B, the total organic carbon removal rate is consistent with the MB photodegradation rate, this proves that MB can be decomposed under the catalyst and visible light, the benzene ring was opened up, also the decrease of total carbon could be caused by the formation of small molecules such as CO<sub>2</sub> and H<sub>2</sub>O.



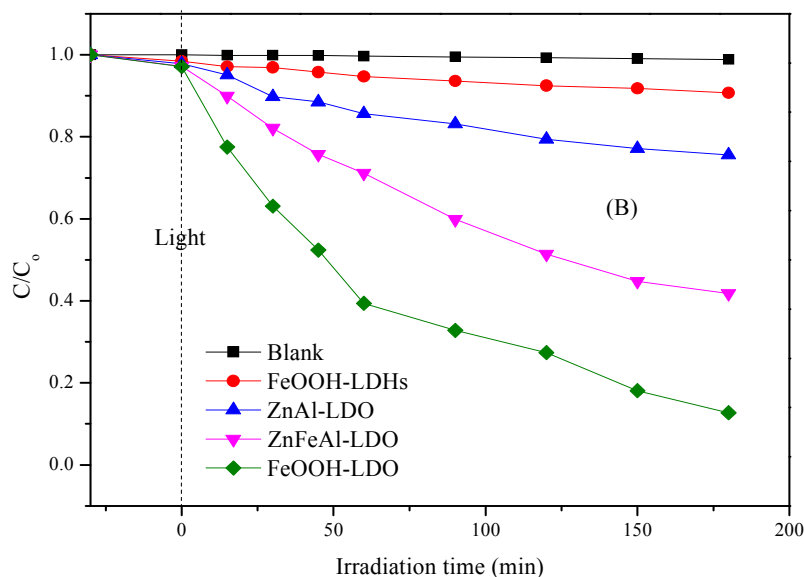


**Figure 5** The photodegradation curves of Methylene blue (A) and total organic carbon concentration (B) by different photocatalysts under visible-light irradiation.

Moreover, UV-vis diffuse reflectance spectra (DRS) of the catalysts were also used to determine the band gap, as shown in Figure 6. We can see that the band gap of FeOOH-LDO was about  $\sim 1.98$  eV. This value is smaller than that of ZnFeAl-LDO ( $\sim 2.25$  eV), ZnAl-LDO ( $\sim 3.02$  eV) and CF ( $\sim 2.01$  eV). The narrow band gap could consume low energy for the electron-hole transition between valence and conduction band [27–29]. In addition, other factors such as crystallite and high specific surface area (providing strong adsorption ability toward the target molecules and thus the generation of photoinduced electron-hole pairs of active sites are enhanced) of photo-catalysts may also attribute to its high photocatalytic activity [30–32].

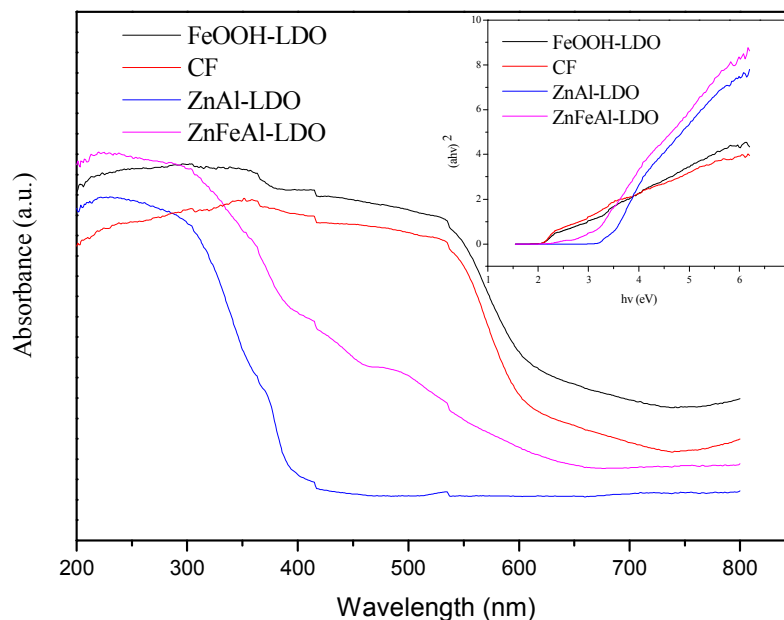


**Figure 6** UV-vis DRS for FeOOH-LDO, ZnFeAl-LDO and ZnAl-LDO. The inset shows their corresponding plots of  $(ah\nu)^2$  vs  $h\nu$  for the determination of the direct band gap.

The improvement of photocatalytic performance of FeOOH-LDO was mainly due to the inclusion of  $\text{ZnFe}_2\text{O}_4$  spinel in FeOOH-LDO material. The first reason is the narrow band gap of  $\text{ZnFe}_2\text{O}_4$  would extend the visible light responsiveness to high wavelength region of the composite. Another one is that  $\text{ZnFe}_2\text{O}_4$  could further protect the photo-chemically vulnerable other major oxides ( $\text{ZnO}$ ,  $\text{Al}_2\text{O}_3$ ,  $\text{Fe}_2\text{O}_3$ ) in FeOOH-LDO composite oxide [33]. Because, several articles reported that the conduction band of  $\text{ZnFe}_2\text{O}_4$  is more negative than that of other major oxides ( $\text{ZnO}$ ,  $\text{Al}_2\text{O}_3$ ,  $\text{Fe}_2\text{O}_3$ ) in FeOOH-LDO composite oxide, whereas the valence band of other

major oxides (ZnO, Al<sub>2</sub>O<sub>3</sub>, Fe<sub>2</sub>O<sub>3</sub>) is more positive than that of ZnFe<sub>2</sub>O<sub>4</sub> in FeOOH-LDO. When irradiated with visible light, the photo-induced electrons tend to migrate to the photochemically more active major oxides (ZnO, Al<sub>2</sub>O<sub>3</sub>, Fe<sub>2</sub>O<sub>3</sub>) domain to affect the reduction of proton for the degradation of MB, while the photo-induced holes tend to migrate to the photochemically stable ZnFe<sub>2</sub>O<sub>4</sub> spinel and subsequently consumed by the oxidation of the reductant in solution [34–36].

### *3.3 Identification of degradation product*

The degradation products of MB (degraded by FeOOH-LDO) have been studied in this research, which was shown in Figure 7.

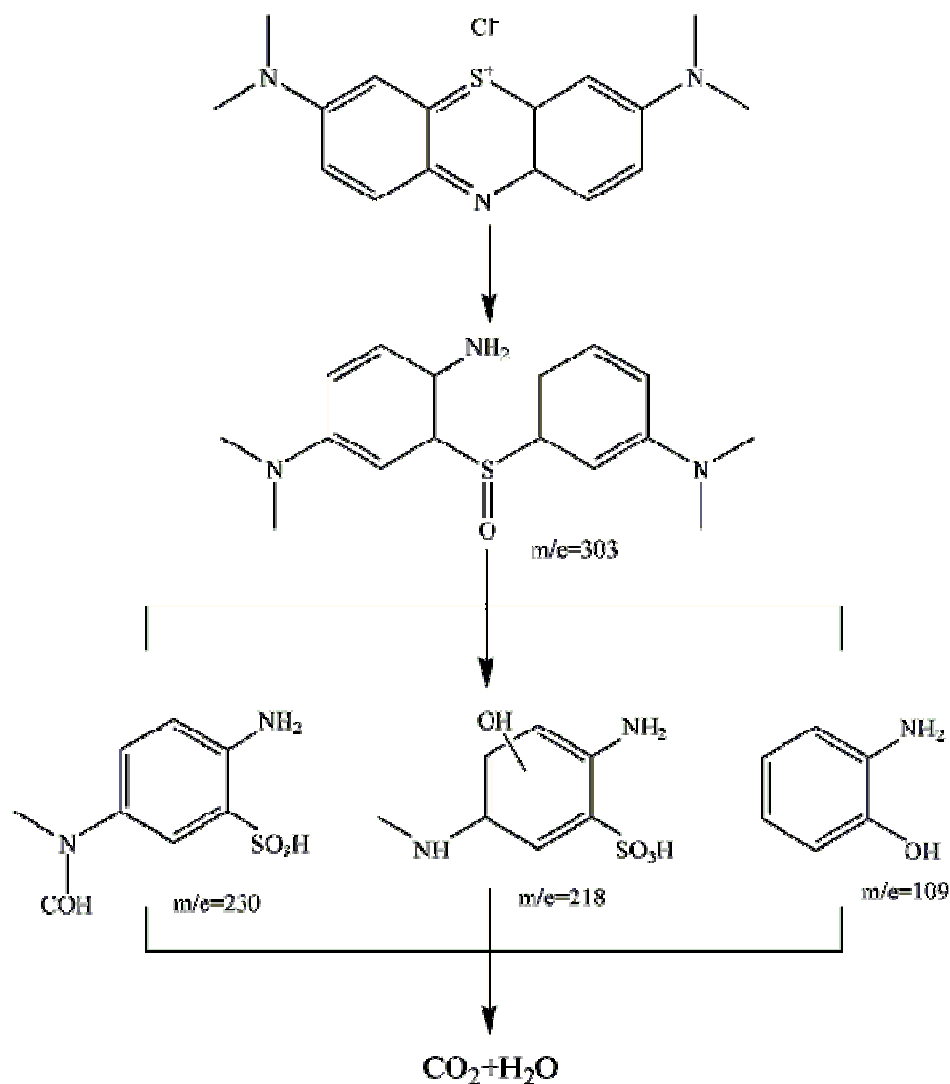


**Figure 7** Decomposition pathway assumed for MB degradation.

First of all (shown in Figure 8), the  $\text{HO}\cdot$  radicals can attack the  $\text{C}-\text{S}^+=\text{C}$  functional group in MB, which is in direct coulombic interaction with  $\text{FeOOH-LDO}$ 's surface. The sulfoxide was identified by LC/MS (supply in supplement materials) at  $m/e=303$ . The electrophilic attack of  $\text{HO}\cdot$  concerned the free doublet of heteroatom S, making its oxidation degree passing from  $-2$  to  $0$ . However, the passage from  $\text{C}-\text{S}^+=\text{C}$  to  $\text{C}-\text{S}(=\text{O})-\text{C}$  requires the conservation of the double bond conjugation, which induces

the opening of the central aromatic ring containing both heteroatoms (S and N). The origin of H atoms necessary to C–H and N–H bond formation can be proposed from the proton reduction by photogenerated electrons as it was already being observed in MB dehydrogenation.

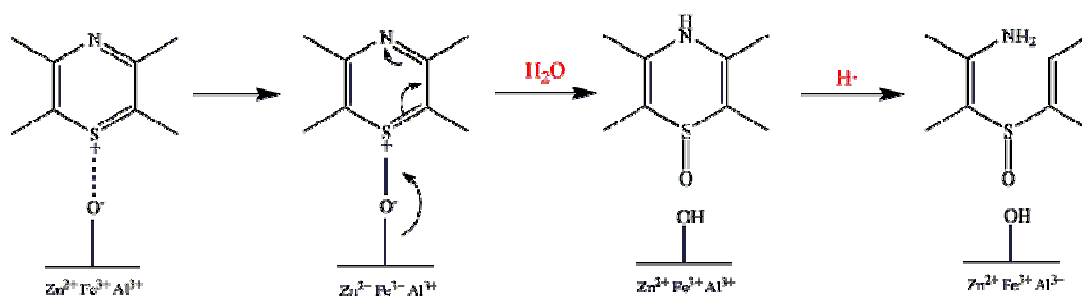


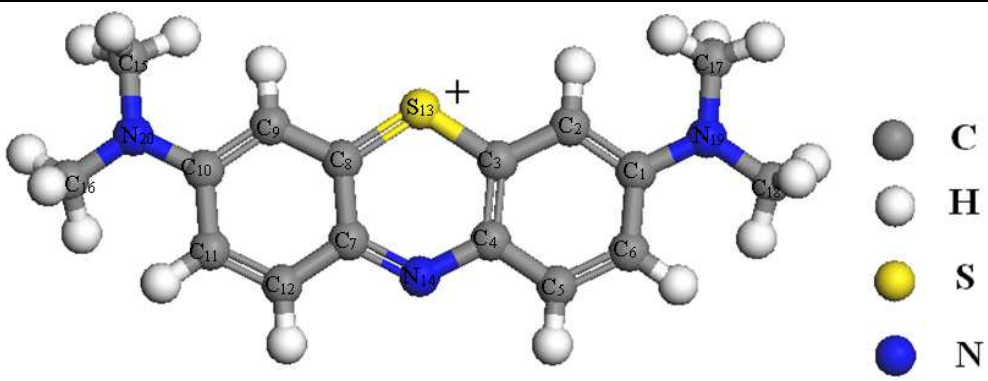
**Figure 8** Electronic reorganization during the passage of MB adsorbed to the sulfoxide form

And then, with the further degradation, the main byproducts of degradation process were 2-Aminophenol, 2-amino-5-(N-methylformamido) benzenesulf acid, and 2-amino-5-(methylamino) hydroxy benzenesulf acid. The mass spectrometry analysis displays  $m/e=109$ , 218 and 230, respectively. Finally, the intermediates could be further decomposed into inorganic micromolecules, like carbon dioxide and water.

In addition, according to Frontier Orbital Theory, positions with higher values of  $2FED^2_{HOMO}$  are more easily subject to electron extraction, higher values of  $FED^2_{HOMO} + FED^2_{LUMO}$  are more attractive for HO• attack [37]. As shown in Table 1, C<sub>4</sub>, C<sub>7</sub> and N<sub>14</sub> sites have the highest  $FED^2_{HOMO} + FED^2_{LUMO}$  value, which implies a higher possibility of mono-hydroxylation formation with HO• attack occurring at

heterocyclic ring. Meanwhile, S<sub>13</sub> position with the lowest  $FED^2_{HOMO} + FED^2_{LUMO}$  value are more easier to obtain electron. Our prediction of the possible sites for hydroxyl addition based on FEDs calculation is in satisfactory agreement with the LC/MS results.

**Table 1** Frontier electron densities on atoms of MB calculated by Gaussian 09 program at the B3LYP/6-311+G\* level.



Atom (number)	$2FED^2_{HOMO}$	$FED^2_{HOMO} + FED^2_{LUMO}$	Atom (number)	$2FED^2_{MO}$	$FED^2_{HOMO} + FED^2_{LUMO}$
C <sub>1</sub>	0.0025	0.0937	C <sub>11</sub>	0.0009	0.0799
C <sub>2</sub>	0.0076	0.0780	C <sub>12</sub>	0.0259	0.0167
C <sub>3</sub>	0.0844	0.0525	S <sub>13</sub>	0.0019	<b>0.0009</b>
C <sub>4</sub>	0.0981	<b>0.2257</b>	N <sub>14</sub>	1.4971	<b>0.7485</b>
C <sub>5</sub>	0.0260	0.0167	C <sub>15</sub>	0.0000	0.0171
C <sub>6</sub>	0.0009	0.0799	C <sub>16</sub>	0.0000	0.0171
C <sub>7</sub>	0.0981	<b>0.2258</b>	C <sub>17</sub>	0.0000	0.0171
C <sub>8</sub>	0.0844	0.0525	C <sub>18</sub>	0.0000	0.0171
C <sub>9</sub>	0.0076	0.0780	N <sub>19</sub>	0.0002	0.0217
C <sub>10</sub>	0.0025	0.0934	N <sub>20</sub>	0.0002	0.0216

#### 4. Conclusions

The good crystal structure of precursor LDH and composite oxides can be successfully synthesized by sol-gel method. The decomposition of MB by the

FeOOH–LDO (inclusion of  $\text{ZnFe}_2\text{O}_4$  spinel) reaches 95% over 180 min, comparative to ~60%, ~23% and ~10% by the samples with ZnFeAl–LDO, ZnAl–LDO and CF, respectively. Moreover, methylene blue could be oxidized into intermediates of 2–Aminophenol, 2–amino–5–(N–methylformamido) benzenesulf acid, and 2–amino–5–(methylamino) hydroxy benzenesulf acid by the hydroxyl radicals ( $\text{OH}\cdot$ ); and finally, the intermediates could be further decomposed into carbon dioxide and water. In addition, frontier electron densities on atoms of MB molecules were also calculated, which in satisfactory agreement with the possible mechanism. Hence, this work demonstrates that the synthesized FeOOH–LDO composite oxides with rather high photocatalytic activity and could be potentially applied in the field of dyes removal.

## References

- [1] W.T. Tsai, C.Y. Chang, M.C. Lin, S.F. Chien, H.F. Sun, M.F. Hsieh, *Chemosphere*, 2001, **45**, 51–58.
- [2] Q.J. Xiang, J.G. Yu, M. Jaroniec, *Chem. Soc. Rev.*, 2012, **41**, 782–796.
- [3] Z.C. Kadirova, K. Katsumata, T. Isobe, N. Matsushita, A. Nakajima and K. Okada, *Appl. Surf. Sci.*, 2013, **284**, 72–79.
- [4] J. Iskra, S. Stavber, M. Zupana, *Tetrahedron Lett.*, 2008, **49**, 893–895.
- [5] S.J. Xia, F.X. Liu, Z.M. Ni, J.L. Xue, P.P. Qian, *J Colloid Interf. Sci.*, 2013, **407**, 195–200.

- [6] Z.M Ni, S.J Xia, L.G. Wang, F.F. Xing, G.X. Pan, *J Colloid Interf. Sci.*, 2007, **316**, 284–291.
- [7] A. Houas, H. Lachheb, M. Ksibi, E. Elaloui, C. Guillard, J.M. Herrmann, *Appl. Catal. B*, 2001, **31**, 145–157.
- [8] B. Liu, H.M. Chen, C. Liu, S.C. Andrews, C. Hahn, P.D. Yang, *J. Am. Chem. Soc.*, 2013, **135**, 9995–9998.
- [9] M. Liu, X.Q. Qiu, M. Miyauchi, K. Hashimoto, *J. Am. Chem. Soc.*, 2013, **135**, 10064–10072.
- [10] S.J. Park, J.P. Lee, J.S. Jang, H. Rhu, H. Yu, B.Y. You, C.S. Kim, K.J. Kim, Y.J. Cho, S Baik, W. Lee, *Nanotechnology*, 2013, **24**, 295202–295212.
- [11] A. Sarkar, A. Shchukarev, A.R. Leino, K. Kordas, J.P. Mikkola, P.O. Petrov, E.S. Tuchina, A.P. Popov, M.E. Darwin, M.C. Meinke, J. Lademann, W. Tuchin, *Nanotechnology*, 2012, **23**, 475711–475718.
- [12] O. Yayapao, T. Tongtem, A. Phuruangrat, S. Thongtem, *J. Alloy. Compd.*, 2013, **576**, 72–79.
- [13] M. Lee, K. Yong, *Nanotechnology*, 2012, **23**, 194014–194019.
- [14] Y. Zhi, Y.G. Li, Q.H. Zhang, H.Z. Wang, *Langmuir*, 2010, **26**, 15546–15553.
- [15] S.J. Xia, Z.M. Ni, Q. Xu, B.X. Hu, J. Hu, *J. Solid State. Chem.*, 2008, **181**, 2610–2619.
- [16] Q. Wang, D. O'Hare, *Chem. Rev.*, 2012, **112**, 4124–4155.
- [17] J.S. Valente, F. Tzompantzi, J. Prince, *Appl. Catal. B*, 2011, **102**, 276–285.

- [18] C.G. Silva, Y. Bouizi, V. Fornés, H. García, *J. Am. Chem. Soc.*, 2009, **131**, 13833–13839.
- [19] M. Wang, L. Sun, J.H. Cai, P. Huang, Y.F. Su, C.J. Lin, *J. Mater. Chem. A*, 2013, **1**, 12082–12087.
- [20] J. Liu, G.K. Zhang, *Phys. Chem. Chem. Phys.*, 2014, **16**, 8178–8192.
- [21] T.H. Yu, W.Y. Cheng, K.J. Chao, S.Y. Lu, *Nanoscale*, 2013, **5**, 7356–7360.
- [22] A. Hamza, H.A. Mohammed, S.M. Waziri, *J. Appl. Sci. Environ. Sanitation*, 2013, **8**, 225–230.
- [23] A. Mantilla, F. Tzompantzi, J.L. Fernández, J.A.I. Díaz Góngora, R. Gómez, *Catal. Today*, 2010, **150**, 353–357.
- [24] K.M. Parida, N. Baliarsingh, B. Sairam Patra, J. Das, *J. Mol. Catal. A: Chem.*, 2007, **267**, 202–208.
- [25] M.F. Shao, J.B. Han, M. Wei, D.G. Evans, X. Duan, *Chem. Eng. J.*, 2011, **168**, 519–524.
- [26] P.P. Qian, J.L. Xue, G.X. Pan, Y. Li, Z.M. Ni, *Chin. J. Inorg. Chem.*, 2012, **28**, 1348–1352.
- [27] J. Wu, W. Walukiewicz, W. Shan, K.M. Yu, J.W. Ager, E.E. Haller, W.J. Schaff, *Phys. Rev. B*, 2002, **66**, 201403(R).
- [28] M.A. Woo, T.W. Kim, I.Y. Kim, S.J. Hwang, *Solid State Ionics*, 2013, **182**, 91–97.
- [29] S.M. Jenekhe, *Nature*, 1986, **322**, 345–347.
- [30] S.Y. Chae, M.K. Park, S.K. Lee, T.Y. Kim, S.K. Kim, W.I. Lee, *Chem. Mater.*, 2003, **15**, 3326–3331.

- [31] M.A. Carreon, S.Y. Choi, M. Mamak, N. Chopra, G.A. Ozin, *J. Mater. Chem.*, 2007, **17**, 82–89.
- [32] S.Y. Chae, M.K. Park, S.K. Lee, T.Y. Kim, S.K. Kim, W.I. Lee, *Chem. Mater.*, 2003, **15**, 3326–3331.
- [33] X.F. Zhao, L. Wang, X. Xu, X.D. Lei, S.L. Xu, F.Z. Zhang, *Amer. Inst. Chemical Engineers*, 2012, **58**, 573–582.
- [34] R. Shao, L. Sun, L.Q. Tang, Z.D. Chen, *Chem. Eng. J.*, 2013, **217**, 185–191.
- [35] A. Goyal, S. Bansal, S. Singhal, *Int. J. Hydrogen Energ.*, 2014, **39**, 4895–4908.
- [36] Y. Hou, X.Y. Li, Q.D. Zhao, G.H. Chen, *Appl. Catal. B*, 2013, **142–143**, 80–88.
- [37] T. An, H. Yang, G.Y. Li, W.H. Song, J. Cooper William, X.P. Nie, *Appl. Catal. B*, 2009, **94**, 288–294.

### Figure Captions

**Figure 1** (A) Power XRD patterns for ZnAl-LDHs, ZnFeAl-LDHs, FeOOH-LDHs and FeOOH; (B) Power XRD patterns for ZnAl-LDO, ZnFeAl-LDO and FeOOH-LDO.

**Figure 2** SEM images for FeOOH (A), CF (B), FeOOH-LDHs (C) and FeOOH-LDO (D). FeOOH-LDHs with high-magnification (E). The corresponding EDX spectrum of the FeOOH-LDO (F).

**Figure 3** N<sub>2</sub> sorption isotherms and pore size distribution of FeOOH-LDO.

**Figure 4** Absorption changes of MB during the photo-degradation process over FeOOH-LDO catalyst under visible-light irradiation.

**Figure 5** The photodegradation curves of Methylene blue (A) and total organic carbon concentration (B) by different photocatalysts under visible-light irradiation.

**Figure 6** UV-vis DRS for FeOOH-LDO, ZnFeAl-LDO and ZnAl-LDO. The inset shows their corresponding plots of  $(ah\nu)^2$  vs  $h\nu$  for the determination of the direct band gap.

**Figure 7** Decomposition pathway assumed for MB degradation.

**Figure 8** Electronic reorganization during the passage of MB adsorbed to the sulfoxide form

### Table Captions

**Table 1** Frontier electron densities on atoms of MB calculated by Gaussian 09 program at the B3LYP/6-311+G\* level.